

Current-driven skyrmion motion in granular films

Xin Gong,¹ H. Y. Yuan,^{2,*} and X. R. Wang^{1,3,†}

¹*Physics Department, The Hong Kong University of Science and Technology, Clear Water Bay, Kowloon, Hong Kong*

²*Department of Physics, Southern University of Science and Technology, Shenzhen 518055, Guangdong, China*

³*HKUST Shenzhen Research Institute, Shenzhen 518057, China*

(Dated: November 5, 2019)

Current-driven skyrmion motion in random granular films is investigated with interesting findings. For a given current, there exists a critical disorder strength below which its transverse motion could either be boosted below a critical damping or be hindered above the critical damping, resulting in current and disorder dependences of skyrmion Hall angle. The boosting comes mainly from the random force that is opposite to the driving force (current). The critical damping depends on the current density and disorder strength. However, the longitudinal motion of a skyrmion is always hindered by the disorder. Above the critical disorder strength, skyrmions are pinned. The disorder-induced random force on a skyrmion can be classified as static and kinetic ones, similar to the friction force in the Newtonian mechanics. In the pinning phase, the static (pinning) random force is transverse to the current density. The kinetic random force is opposite to the skyrmion velocity when skyrmions are in motion. Furthermore, we provide strong evidences that the Thiele equation can perfectly describe skyrmion dynamics in granular films. These findings provide insight to skyrmion motion and should be important for skyrmiontronics.

I. INTRODUCTION

Magnetic skyrmions have attracted much attention in recent years because of their potential applications in information storage and processing, besides their academic interest^{1–46}. This potential can only be realized when a good understanding of disorder effect on skyrmion motion is obtained because defects/inhomogeneity exist inevitably in all materials. There are a few studies^{36–48} of skyrmion in disordered systems. Many phenomena were observed with limited understanding. For example, in the presence of isolated impurities, micromagnetic simulations suggest that skyrmions sometimes avoid impurities³⁷ and sometimes be trapped by disorders⁴⁰. There is no well-accepted understanding of these seemingly conflicting results. The ability of a skyrmion to avoid trapping with detoured trajectory away from isolated defects was attributed to its topological property³⁷. This interesting ability leads to the theoretical prediction³⁷ that disorders have little effects on skyrmion driving current density. Just like their counterparts in a uniform film, skyrmions in a disordered film should move under a current density as low as $10^5 - 10^6$ A/m², five orders of magnitudes smaller than that for a domain wall³⁷. However, the experimental reported driven current is above $10^{10} - 10^{11}$ A/m^{2,32,34,36}, not too far from the typical magnetic domain wall driving current and far above the community's expectation. Skyrmions can also perform a random-walk-like motion in disordered system⁴⁹. All these issues and more need detail analysis and a better understanding.

In this paper, we study the influences of disorders on skyrmion motion. Our numerical and analytical results show that disorder could boost skyrmion transverse motion under certain conditions while disorders always hinder skyrmion longitudinal motion. Thus, the skyrmion Hall angle increases in the disorder system. The physics

behind the boosting (hindering) of the transverse (longitudinal) motion is mainly from the random forces along the driving force direction: When the random force is opposite to the driving force, skyrmion transverse speed increases while the longitudinal speed decrease. In the opposite case when the random force is along the driving force, the transverse speed decreases and the longitudinal speed increase. As a result, the duration time of the skyrmion with a larger (smaller) transverse (longitudinal) speed is longer than that in the opposite situation. This explains boosting of the time average transverse skyrmion speed and the hindering of the average longitudinal speed in disorders. In comparison, the random force transverse to the current direction decreases or increases both skyrmion transverse and longitudinal speeds at the same time. To the first order, the random force in the transverse direction has little effect on average skyrmion velocity.

The paper is organized as follows. In Sec. II, we first describe the model and approach adopted in this study. Sec. III presents our main findings, including three phases, origin of the boosting of skyrmion transverse motion, static and kinetic random forces, and how accurate the Thiele equation is in describing skyrmion motion in granular films. Interestingly, the average random force on a moving skyrmion is opposite to the skyrmion velocity. In the discussion, we point out the fundamental differences between disorder-induced domain wall motion boosting and skyrmion motion boosting, and show that the physics presented here does not change when the non-adiabatic torque is present as long as its value is smaller than the damping coefficient. We will also discuss the spin-orbit torque driven skyrmion motion. The conclusion is given in Sec. IV, followed by Acknowledgements.

II. MODEL AND METHODOLOGY

We consider a perpendicularly-magnetized random granular film that is constructed by a Voronoi tessellation, as shown in Fig. 1(a). Magnetic anisotropy K in each grain is randomly distributed around $K_0 = 8.0 \times 10^5$ J/m³ either with a Gaussian distribution of deviation ΔK or in a window of $(K_0 - \Delta K, K_0 + \Delta K)$. The granular film with Gaussian distribution is assumed below if it is not specified.

The material parameters are chosen in such a way that supports a stable isolated skyrmion²⁴. Initially, a skyrmion is located in the center (also the origin of the xyz -coordinate). Spin dynamics is governed by the Landau-Lifshitz-Gilbert (LLG) equation,

$$\frac{\partial \vec{m}}{\partial t} = -\gamma \vec{m} \times \vec{H}_{\text{eff}} + \alpha \vec{m} \times \frac{\partial \vec{m}}{\partial t} + \vec{\tau}, \quad (1)$$

where \vec{m} , γ , α are respectively the unit vector of the magnetization, gyromagnetic ratio, and the Gilbert damping. $\vec{H}_{\text{eff}} = 2A\nabla^2 \vec{m} + 2Km_z \hat{z} + \vec{H}_d + \vec{H}_{\text{DM}}$ is the effective field including the exchange field characterized by the exchange stiffness A , crystalline anisotropy field along the z -direction, dipolar field \vec{H}_d , and the Dzyaloshinskii-Moriya interaction (DMI) field \vec{H}_{DM} characterized by DMI coefficient D . In this study, we consider the interfacial DMI with DMI energy density of $D[(\hat{z} \cdot \vec{m})\nabla \cdot \vec{m} - (m \cdot \nabla)(\hat{z} \cdot \vec{m})]$. $\vec{\tau} = -(\vec{u} \cdot \nabla)\vec{m} + \beta \vec{m} \times (\vec{u} \cdot \nabla)\vec{m}$ is the spin transfer torque consisting of a damping-like torque and a field-like torque^{50,51}, where β is a dimensionless coefficient measuring the strength of the field-like torque and $\vec{u} = \vec{J}P\mu_B/(eM_s)$ is of a quantity of dimension of speed measuring amount of equivalent magnetic moments supplied from spin polarised current to the magnet per unit time. Here J, P, μ_B, e , and M_s are respectively current density, current polarization, the Bohr magneton, the electron charge, and the saturation magnetization. To study the skyrmion dynamics, we use the Mumax3 package⁵² to numerically solve the LLG equation on the granular film of size of 1024 nm \times 512 nm \times 1 nm. The mesh size is 1 nm \times 1 nm \times 1 nm. This choice of mesh size is tested through the non-change in simulation results when a smaller mesh size is used (See Appendix for the results of smaller mesh size). The average grain size is of 5 nm, and the model parameters are $A = 15 \times 10^{-12}$ J/m, $D = 0.003$ J/m², $M_s = 5.8 \times 10^5$ A/m in this study.

To understand the skyrmion dynamics, we derive the Thiele equation in disorders by considering $\partial_i \vec{m} \cdot (\vec{m} \times \text{Eq. (1)})$. Under the rigid-body assumption and after some algebras, we obtain following equation for skyrmion-velocity \vec{v}

$$\vec{G} \times (\vec{v} - \vec{u}) + \vec{D} \cdot (\alpha \vec{v} - \beta \vec{u}) + \frac{\gamma}{M_s d} \nabla E = 0, \quad (2)$$

where d is the film thickness, $\vec{G} = G\hat{z} = 4\pi Q\hat{z}$ is the skyrmion gyrovector proportional to the skyrmion number Q ²⁴, and the tensor $D_{ij} = \int \partial_i \vec{m} \cdot \partial_j \vec{m} dS$ is the

dissipation dyadic. For symmetric skyrmion structures, $D_{ij} = D\delta_{ij} = \frac{1}{2}(R/w + w/R)\delta_{ij}$ where R and w are respectively skyrmion size and skyrmion wall width²⁴. $E(\vec{R}) = \int \int \{A(\nabla \vec{m})^2 + D[(\hat{z} \cdot \vec{m})\nabla \cdot \vec{m} - (m \cdot \nabla)(\hat{z} \cdot \vec{m})] - K(\vec{x}, \vec{y})m_z^2\} dxdy$ is the total energy of a skyrmion centred at position \vec{R} . In a homogeneous film, the total energy of the skyrmion does not depend on the skyrmion position ($\nabla E = 0$) due to the translational symmetry of the system. Eq. (2) is the original equation derived by Thiele.⁵³ In a granular film, the translational symmetry breaks so that $\nabla E \neq 0$. $\vec{F} \equiv -\frac{\gamma}{M_s d} \nabla E$ is a random force in all directions when a skyrmion is in motion. At the moment, we set $\beta = 0$ and $\vec{F} = (F_x, F_y)$ and Eq. (2) becomes,

$$Gv_x + \alpha Dv_y = Gu + F_y \quad (3a)$$

$$Gv_y - \alpha Dv_x = -F_x \quad (3b)$$

Without losing generality, we set $Q = 1$ and assume $u > 0$. The solution of the above skyrmion dynamical equations is $v_x = [G^2 u + GF_y + \alpha DF_x]/[G^2 + (\alpha D)^2]$, $v_y = [\alpha DG u + \alpha DF_y - GF_x]/[G^2 + (\alpha D)^2]$. In a homogeneous film, we have $F_x = F_y = 0$ and $v_y > 0$ and $0 < v_x < u$ since $\alpha D > 0$. Furthermore, the skyrmion Hall angle does not depend on u (current). For a negative (positive) F_x and $F_y = 0$, v_y increases (decreases) and v_x decreases (increases), skyrmion Hall angle depends on both disorders and u . In contrast, v_x and v_y vary with F_y differently when $F_x = 0$: v_x and v_y increase (decrease) simultaneously for $F_y > 0$ ($F_y < 0$). These dependences of v_x and v_y are important for us to understand the boosting of skyrmion transverse discussed below.

III. RESULT

A. Three Phases

Figures 1(b) and 1(c) plot skyrmion positions $\vec{R} = (x_c, y_c)$ as a function of time for a homogeneous film (black squares) and for a granular film (red dots) of $\Delta K = 3\%K_0$ for $\alpha = 0.3$, $\beta = 0$, $J = 6 \times 10^{11}$ A/m². x_c and y_c for the granular film are the ensemble average over 10 independent realizations. The inset shows the position differences of three typical granular films and the homogeneous film. The trajectory of skyrmion motion in the homogeneous film is a perfectly straight line with constant velocity, while it wiggles around a straight line in each realization of random granular film as shown in the insets. The ensemble average of $x_c(t)$ and $y_c(t)$ are perfectly linear so that average skyrmion velocity \vec{v} is a good description of skyrmion motion. The average longitudinal and transverse skyrmion velocities are $v_x = 19.7$ m/s and $v_y = 8.9$ m/s for random granular films, $v_x = 20.7$ m/s and $v_y = 8.0$ m/s for the homogeneous film, which agree perfectly with solution of Eq. (2) with $\nabla E = 0$ (black lines). Interestingly, the transverse

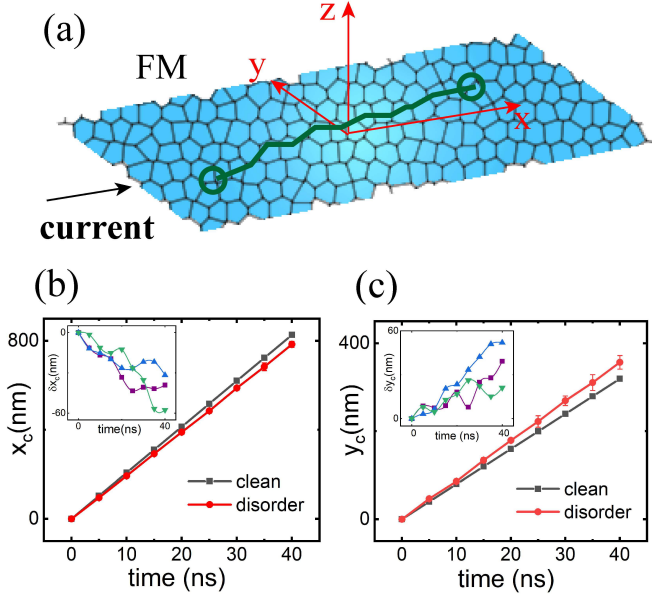


FIG. 1. (color online) (a) Schematic illustration of a skyrmion in a granular chiral magnetic film with randomly distributed anisotropy. (b) and (c) Time evolution of 10 ensemble averaged skyrmion position $\vec{R} = (x_c, y_c)$ under an electric current for a granular film of $\Delta K = 3\%K_0$ (red dots). For a comparison, black squares are for a homogeneous film. The inset shows the position difference between the homogeneous and three typical granular films. The three curves are for three different realizations. The model parameters are $\alpha = 0.3$, $\beta = 0$, $J = 6 \times 10^{11} \text{ A/m}^2$.

motion is boosted by the disorder while the longitudinal motion is hindered.

One can compute the average skyrmion velocity and its statistical errors from different realizations and for different disorder strengths and Gilbert damping. Fig. 2 shows how averaged v_y and its error bar with the disorder strength $\Delta K/K_0$ (in percentage) for current density $J = 6 \times 10^{11} \text{ A/m}^2$ and $\alpha = 0.6$ (a) and $\alpha = 0.3$ (b). Points of zero velocity correspond to the skyrmion pinning, similar to the magnetic domain wall pinning by disorders or notches^{54–56}. The critical disorder strength, above which all skyrmion are pinned, depends on the current density J (proportional to u). In cyan region, the average transverse velocity in the granular film is larger than that in the homogeneous film, and system is in the boosting phase. As disorder strength $\Delta K/K_0$ increases, the error bars increase and the average transverse velocities in disorder systems increase parabolic for $\alpha = 0.3$. For a larger disorder strength $\Delta K/K_0 > 4\%$, the skyrmions are in pinning phase (red region). The inset shows a linearly J -dependence of the critical disorder $\Delta K/K_0$, like the effect of the friction force in a Newtonian mechanics that one needs a larger driven force to maintain the motion of a body on a rougher surface. The physics does not depend on whether the distribution function of random K is Gaussian or uniform in a win-

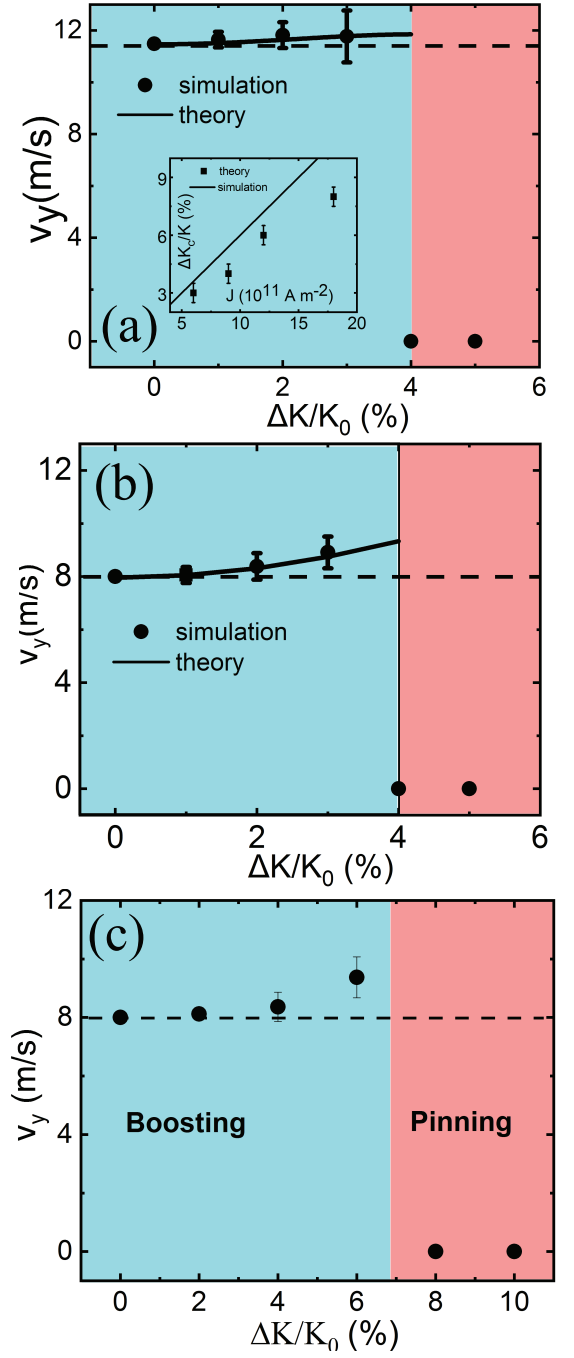


FIG. 2. (color online) Disorder strength dependence of skyrmion transverse velocity for $J = 6 \times 10^{11} \text{ A/m}^2$. (a) and (b) are for Gaussian distribution of magnetic anisotropy with $\alpha = 0.6$ (a) and $\alpha = 0.3$ (b). (c) is the same plot for the uniform distribution of magnetic anisotropy with $\alpha = 0.3$. The horizontal dashed line is v_y of the homogeneous film while dots are simulation results and the solid line is the solution of Eqs. (2) and (4) for $\beta = 0$ with a fitting parameter b defined in random force f . The cyan and red colors denote the boosting phase and pinning phase, respectively. The inset shows the critical disorder strength as a function of the current density for $\alpha = 0.3, \beta = 0$, the black squares are numerical results.

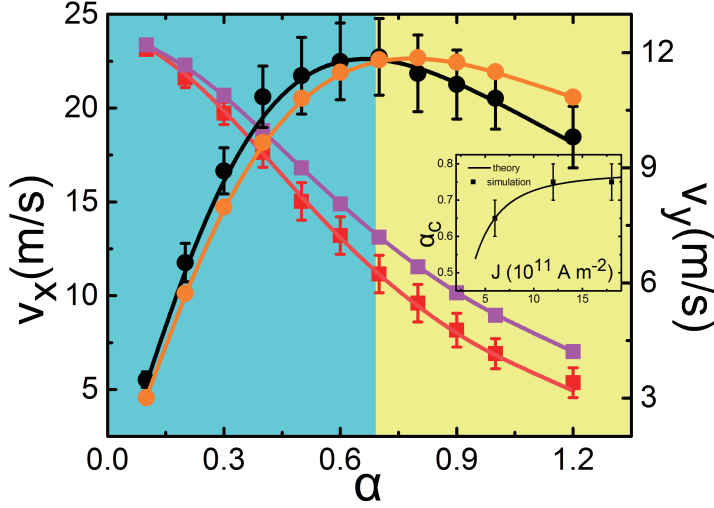


FIG. 3. (color online) The α -dependence of longitudinal (squares) and transverse (dots) velocities for $J = 6 \times 10^{11} \text{ A/m}^2$ and $\Delta K = 3\%K_0$. The orange and magenta colors denote the velocities in the homogeneous film while the black and red colors are for the granular film. The lines are the solutions of Eqs. (2) and (4) with b in f (for granular film) as a fitting parameter. The cyan and yellow colors denote the boosting phase and hindering phase, respectively. The inset shows the current density dependence of critical damping. Other parameters are $\beta = 0$ and those specified in the model.

dow. As shown in Fig. 2(c) for K uniformly distributed in a window of $[K_0 - \Delta K, K_0 + \Delta K]$, one can clearly see both boosting and pinning. The only difference is at qualitative level.

Fig. 3 shows how v_x (squares) and v_y (dots) change with the Gilbert damping coefficient α for $J = 6 \times 10^{11} \text{ A/m}^2$, $\beta = 0$, and $\Delta K = 3\%K_0$. Different from v_x that monotonically decreases with α (red), v_y (black) increases first and then decreases with α as shown in Fig. 3. To see boosting and hindering effect, we have also plotted v_x and v_y for the homogeneous film (orange and magenta respectively) for the same model parameters. Obviously, skyrmion transverse motion is boosted (hindered) by the disorder for $\alpha < 0.7$ ($\alpha > 0.7$). Interestingly, the critical damping that separates boosting from hindering coincides with the peak position of v_y . The longitudinal motion is, however, always hindered by the disorder in our simulations. The value of the critical damping coefficient depends on the current density as shown in the inset.

In summary, three phases are identified: Pinning phase above the critical disorder strength; boosting of skyrmion transverse motion below the critical disorder strength and below a critical damping coefficient; hindering of skyrmion transverse motion below the critical disorder strength and above the critical damping. Both critical disorder strength and critical damping coefficient depend on the applied current density and other model pa-

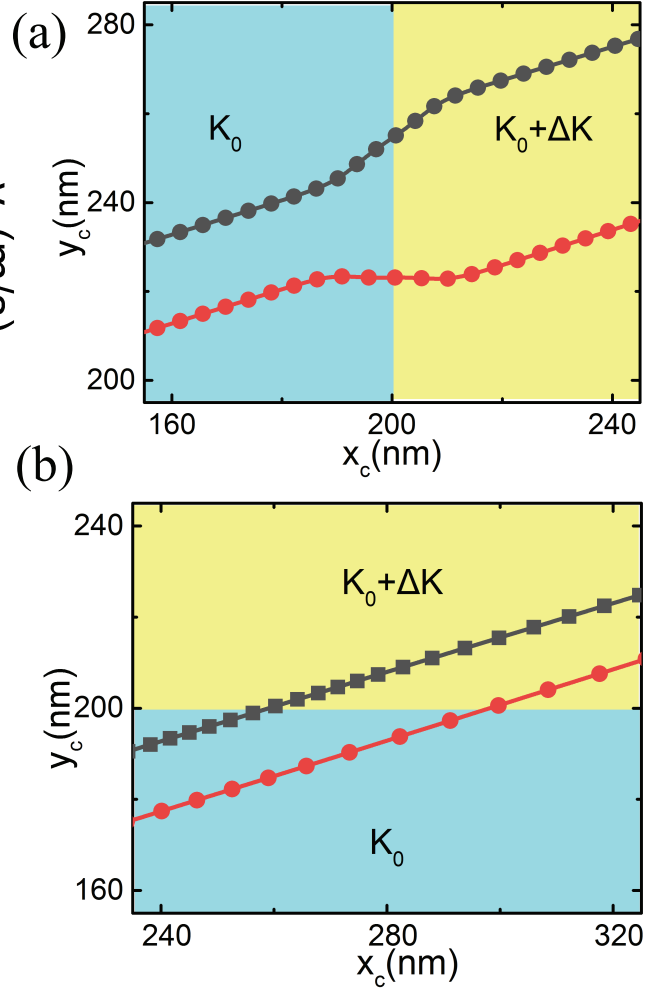


FIG. 4. (color online) Model parameters in this figure are $J = 6 \times 10^{11} \text{ A/m}^2$, $\alpha = 0.3$, $\beta = 0$ and $K_0 = 8.0 \times 10^5 \text{ J/m}^3$, as well as those specified in the model. (a) A y -aligned boundary. The anisotropy is K_0 on the left of the boundary, and $K_0 + \Delta K$ on the right of the boundary. The lines indicate the skyrmion trajectories when it cross the boundary from the left. Black lines for $\Delta K = 3\%K_0$ ($F_x < 0$) and red line for $\Delta K = -3\%K_0$ ($F_x > 0$). (b) A x -aligned boundary. The anisotropy is $K_0 + \Delta K$ above the boundary, and K_0 below the boundary. The lines indicate the skyrmion trajectories when it cross the boundary from the bottom. Black line for $\Delta K = 3\%K_0$ ($F_y < 0$) and red line for $\Delta K = -3\%K_0$ ($F_y > 0$).

rameters. Numerically, critical damping α_c at disorder strength $\Delta K_c/K_0 = 3\%$ seems coincide with the peak position of v_y .

B. Origins of Boosting

To understand the origins of the boosting of skyrmion transverse motion, we consider how a skyrmion cross a y -aligned boundary (Fig. 4(a)) and a x -aligned boundary (Fig. 4(b)) that separates two otherwise homogeneous

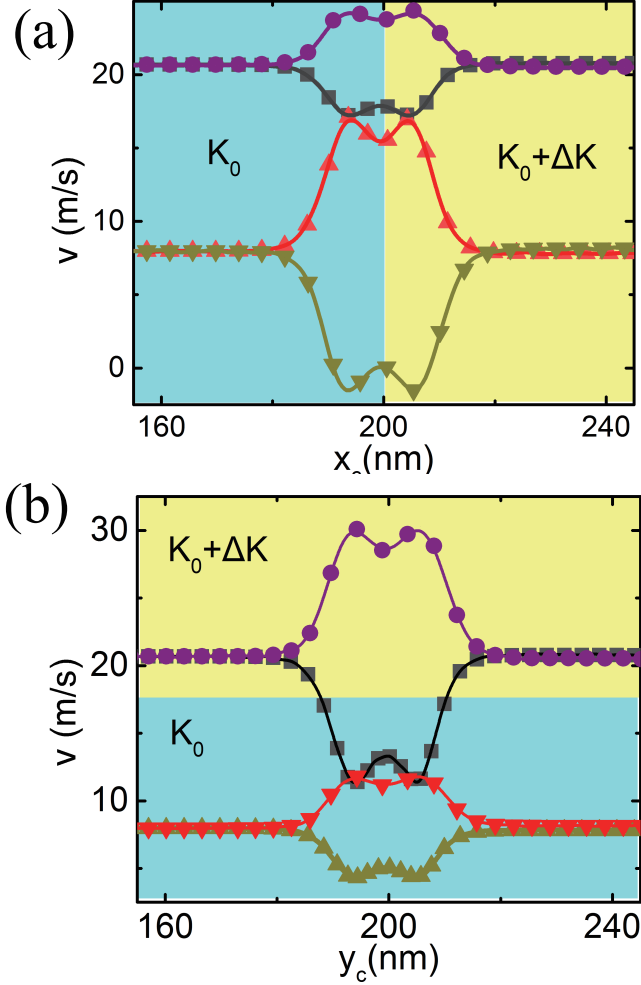


FIG. 5. (color online) Model parameters in this figure are $J = 6 \times 10^{11} \text{ J/m}^2$, $\alpha = 0.3$, $\beta = 0$ and $K_0 = 8.0 \times 10^5 \text{ J/m}^3$, as well as those specified in the model. (a) v_x and v_y at different position for a y-aligned boundary. Squares and up-triangles are of simulations results of v_y and v_x , respectively, for $\Delta K = 3\%K_0$ while dots and down-triangles are of v_y and v_x for $\Delta K = 3 - \%K_0$. (b) v_x and v_y at different position for a x-aligned boundary. Squares and up-triangle are of simulations results of v_x and v_y , respectively, for $\Delta K = 3\%K_0$ while dots and down-triangles are for $\Delta K = -3\%K_0$. All lines in the two figures are numerical solutions of Eq. (2) in which instantaneous E and \vec{D} obtained from skyrmion structure are used.

magnetic films. For a y-aligned boundary, the boundary force on a rightward moving skyrmion is along the positive x-direction, $F_x > 0$, when the magnetic anisotropy of the film on the left is larger than K on the right (all other model parameters are the same as specified early). Fig. 5(a) shows clearly that the average transverse velocity (down-triangles) becomes smaller while the longitudinal velocity (dots) is larger near the boundary. The skyrmion trajectory (red dots and line) is deflected to-

wards x-direction near the boundary as indicated by the red line in Fig. 4(a).

If K on the left is smaller than K on the right, the boundary force is negative, $F_x < 0$, and v_y (up-triangles) is larger near the boundary while v_x (squares) becomes smaller near the boundary shown in Fig. 5(a). Thus, the skyrmion trajectory is deflected towards y-direction near the boundary as indicated by the black dots and line in Fig. 4(a). This feature was also observed by others⁵⁷, and was termed as gliding motion of skyrmions. However, its true origin was not sufficiently revealed. It should be pointed out that all the lines in Fig. 5 are the numerical solutions of Eq. (2) in which E and \vec{D} are numerically computed from the spin structures in simulations that vary with time. The perfect agreement between micromagnetic simulations and numerical solutions of Eq. (2) demonstrates excellent approximation of the Thiele equation although the rigid-body assumption is obviously invalid for a skyrmion cross a boundary. For a randomly distributed disorders, the sizes of regions with $F_x > 0$ and $F_x < 0$ should be the same so that a skyrmion spend more time stay in $F_x < 0$ regions than that in $F_x > 0$ ones. As a result, the time average skyrmion transverse velocity is boosted while the longitude velocity is hindered.

In contrast, when a skyrmion crosses a x-aligned boundary (4(b)), both v_x (dots and squares) and v_y (down-triangles and up-triangles) increase near the boundary for $F_y > 0$ and decrease near the boundary for $F_y < 0$, as shown in Fig. 5(b). Again, the lines in the figures are the numerical solutions of Eq. (2). Different from the effect of F_x , random force in the transverse direction has no much effect on the skyrmion hall angle because it increases (decreases) longitudinal and transverse simultaneously so that skyrmion trajectories show negligible deflection when skyrmions cross the boundary as shown by the red and black lines in Fig. 4(b). From Fig. 5(b), a velocities difference of about 0.1 m/s in the left and right domain far away from the boundary is observed that is much smaller than the boundary effect. Thus, influence of the boundary force dominant and small variation of \vec{D} in different domains will be neglected in the following analysis. Follow the same analysis as the case of F_x , we found weak hindering of both v_x and v_y . In summary, both y-aligned and x-aligned boundary effect lead to the hindering of longitude motion. However, y-aligned boundary effect is the main cause of boosting of transverse motion.

C. Random Force at Pinning and in Motion

In order to have a better understanding of three phases, we would like to consider the random force defined in Eqs. (2) and (3). For simplicity, we consider only the case of $\beta = 0$. When a skyrmion is at rest, then random force should balance the driven force from current \vec{u} , i.e. $\vec{F} = \vec{G} \times \vec{u}$. Thus the static random (pinning) force

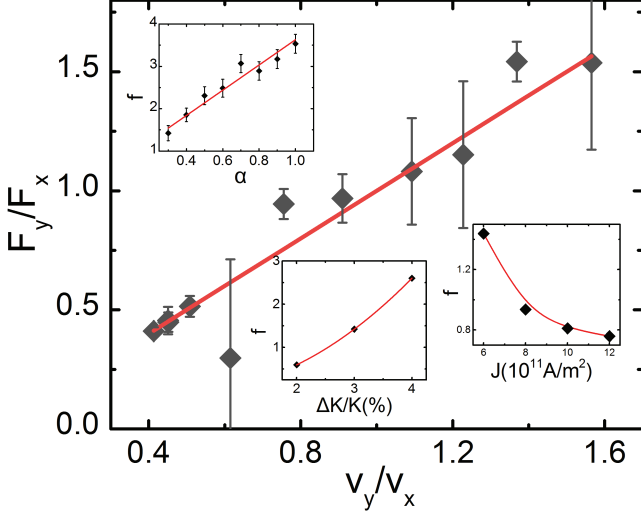


FIG. 6. (color online) F_y/F_x vs. v_y/v_x for various J , ΔK , and α . All other model parameters are specified in the section of model. Filled diamonds are the numerical data, and the black line is for $y = x$. All $(F_y/F_x, v_y/v_x)$ fall around the line. Insets show the f dependence on J , ΔK , and α .

must be transverse to the current direction. To study the random force on a skyrmion when it moves in a random potential landscape, we would like to numerically verify our conjecture that, like the friction force of an object moving on a surface that is always opposite to its velocity in Newtonian mechanics, average random force is also opposite to the skyrmion motion. Since Thiele equation is an excellent description of skyrmion dynamics in domains and crossing domain boundaries, we can substitute the instantaneous skyrmion velocity obtained from the micromagnetic simulations into Eq. (3) to obtain the numerical random force for a given system at each moment. Obviously, this is a stochastic quantity that varies from time to time. In terms of skyrmion motion, the meaningful quantity is the time averaged random force. Below, all F_x and F_y are the time averaged values for each given system. One can obtain different pairs of $(F_y/F_x, v_y/v_x)$ by using different J , α , and ΔK , and they should fall on line $y = x$ if $\vec{F} \parallel -\vec{v}$. Fig. 6 plot points of $(F_y/F_x, v_y/v_x)$ in the $F_y/F_x - (v_y/v_x)$ plane. It is clear that all points of $(F_y/F_x, v_y/v_x)$ lie indeed around line $y = x$, a strong numerical evidence that the direction of \vec{F} is opposite to skyrmion velocity,

$$\vec{F} = -f\hat{v}, \quad (4)$$

where \hat{v} is the unit direction of skyrmion velocity.

f depends on the driven current, disorder strength as well as the skyrmion structure. From Eq. (3), the average velocity $v_x = \frac{G^2 u - (\alpha D F_x)^2 / G^2 u}{G^2 + (\alpha D)^2}$ and $v_y = \frac{\alpha D G u + \alpha D F_x^2 / G u}{G^2 + (\alpha D)^2}$. Assume the regions of $F_x < 0$ and $F_x > 0$ are the same, the time average random force should be $F = F_x(1/v_{x1} - 1/v_{x2})/(1/v_{x1} + 1/v_{x2}) =$

$-F_x(v_{x1} - v_{x2})/(v_{x1} + v_{x2}) \simeq -(\alpha D F_x^2)/G^2 u$, where v_{x2} (v_{x1}) is of the velocity under random force $-F_x$ (F_x). This suggests that f takes the form of $f = b\alpha D \Delta K^2/J = b\alpha D \delta/u$, where $\delta \equiv \Delta K^2 P \mu_B / (e M_s)$ measures disorder strength and has a dimensionality of velocity. b is a dimensionless numerical factor of order of 1. To test this reasoning, we numerically plot f against α , ΔK , and J in the insets of Fig. 6. As shown in the insets, f is proportional to α , ΔK^2 , but inversely proportional to J , as conjectured.

We can test how good of this f is by substituting Eq. (4) into Eq. (3), and solve for \vec{v} as a function of $\Delta K/K$ and αD by treating b as the only fitting parameter. For the small pinning strength ($\Delta K/K_0 \leq 3\%$), we carried out the calculation for the model parameters used for simulations in Figs. 2 and 3, and the lines are the theoretical results. Almost perfect agreement between the simulation results and numerical solution of Eq. (3) demonstrates not only high accuracy of the Thiele equation, but also the excellent approximation of f .

D. Phase Diagram

By substituting \vec{F} in Eq. (4) into the generalized Thiele equation (2), we can solve the equation for skyrmion velocity,

$$v_x = \frac{G^2}{G^2 + (\alpha D + f/v)^2} u \quad (5a)$$

$$v_y = \frac{G(\alpha D + f/v)}{G^2 + (\alpha D + f/v)^2} u \quad (5b)$$

$$v = \frac{\sqrt{(u^2 - f^2)(G^2 + (\alpha D)^2) + \alpha^2 D^2 f^2} - \alpha D f}{G^2 + (\alpha D)^2} \quad (5c)$$

where $v \equiv |\mathbf{v}| = \sqrt{v_x^2 + v_y^2}$. Clearly, Eq. (5a) shows that the longitudinal velocity (v_x) is always hindered by the random force f . Eq. (5b) suggests the existence of a maximum v_y at $\alpha D + f/v = G$, leading to a critical damping $\alpha_c = G/[(1 + \frac{b\Delta K^2}{Jv})D]$ that separate boosting phase from the hindering phase. To pin a skyrmion, the random force proportional to ΔK must balance the driven force of magnitude $G u$. Thus the critical pinning disorder strength should be of $\Delta K_c = c G u$, or $\Delta K_c/J = c P \mu_B / (e M_s)$, where c is a factor that depends on the skyrmion size and structure.

As shown in Fig. 7 in the plane of $\Delta K_c/J - (\alpha D)$, $\Delta K_c/J = c P \mu_B / (e M_s)$ (black line with an optimal c) separates the pinning phase from the unpinned phase, and $\alpha_c = G/[(1 + \frac{b\Delta K^2}{Jv})D]$ (red line) further separate the boosting phase from the hindering phase. Since the boundaries are obtained from the average random force which is smaller than the maximal possible force in the granular film, one should expect the critical disorder strength under-estimate the pinning since it the maximal possible force from the random potential landscape that is relevant for the pinning. Indeed, as one can see the

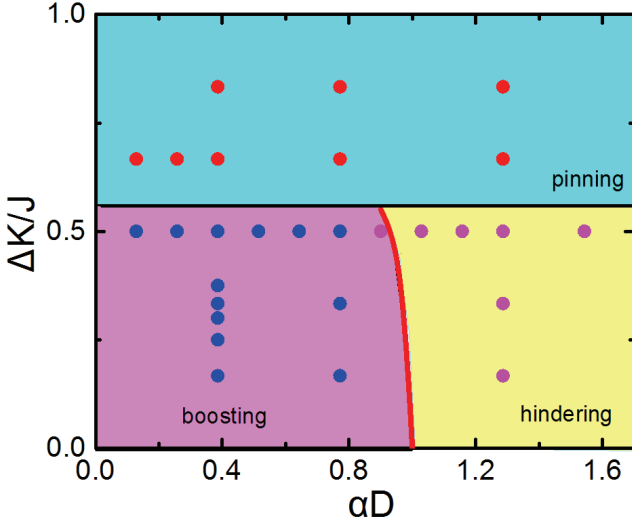


FIG. 7. (color online) Three phases in $\Delta K/J$ - αD plane. Dots are simulations results for pinning (red), boosting (blue) and hindering (pink) phases. The two boundary lines separating three phases. The black line are pinning-unpinning boundary while the red line are boosting-hindering boundary

true simulations results (insets in Fig. 2), pinning occurs at a disorder strength below the theoretical prediction.

From Eq. (5), one can also obtain the skyrmion Hall angle

$$\theta_{SH} = \tan^{-1} \left(\alpha D + \frac{\delta}{u^2} \alpha D \sqrt{1 + \alpha^2 D^2} \right). \quad (6)$$

It predicts that the Hall angle decrease gradually with current density and approaches a constant value αD that is the hall angle for the homogeneous film. As shown in Fig. 8(a), this formula (red line) could well capture the trend of numerical results (dots). The discrepancy may come from the current density dependence of the pinning strength δ and the deformation of moving skyrmion that is not included in our model.

IV. DISCUSSIONS AND CONCLUSIONS

It was known that disorders can also boost magnetic domain wall propagation^{55,56}. The boosting there is related to the generation of anti-vortices that can both help domain wall depinning^{55,56} and exert an extra driving force through Magnus effect. Thus, it is very different from the physics of disorder-boosted transverse skyrmion motion that come from the random force opposite to the current direction. So far, all simulations are for $\beta = 0$. In realistic system, non-adiabatic torque β should not be zero in general although its value is believed to be small. Thus, it is nature to ask whether the physics will be different when non-zero β is considered. To address this issue, we have also carried out the same simulation for non-zero β and the results are shown in Fig. 9. The

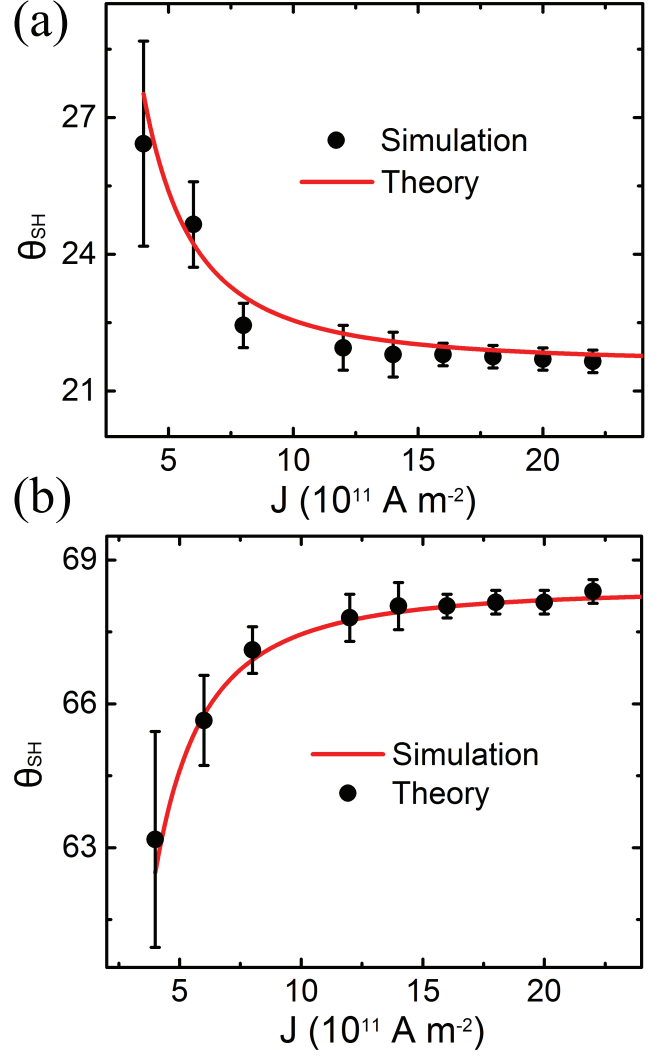


FIG. 8. (color online) The current density dependence of skyrmion Hall angle θ_{SH} for the STT driven (a) and SOT driven (b) cases. Red lines are Eq. (6) and Eq. (8), black circles are numerical results. Other parameters are $\Delta K = 3\%K_0$, $\beta = 0$

longitudinal velocity is always hindered by the disorders regardless of value of β . Note that the transverse velocity reverses its sign at $\beta = \alpha$. Thus, the transverse skyrmion motion is always boosted for $\beta < \alpha$ while the boosting is absent when $\beta > \alpha$. Thus, the main results reported here is valid only when $\beta < \alpha$.

Although our simulations and theory focus on the current-driven skyrmion motion thorough spin transfer torque (STT), all the physics is still valid for skyrmion motion through spin-orbital torque, and the corresponding Thiele equation is^{32,58},

$$\vec{G} \times \vec{v} + \alpha \vec{D} \cdot \vec{v} - \vec{B} \cdot \vec{u}' - \vec{F} = 0, \quad (7)$$

where the element of \vec{B} is $B_{ij} = \iint \int (\partial_i m_z m_j - m_z \partial_i m_j) dx dy$. and $u' = (\gamma \hbar \theta_{SH}) / (2e M_s d)$ The Hall an-

gle from the the new Thiele equation becomes

$$\theta_{\text{SH}} = \pi/2 - \tan^{-1} \left(\alpha D + \frac{\delta}{u^2} \alpha D \sqrt{1 + \alpha^2 D^2} \right). \quad (8)$$

The driving current dependence of skyrmion Hall angle has been observed in both experiments and micromagnetic simulations^{32,34,38}. But, to the best of our knowledge, analytical formula like Eqs. (6) and (8) for the skyrmion Hall angle were not known.

Figure 8(b) is of the comparison of our theory with the micromagnetic simulations (dots). Different from the STT-driven case, the Hall angle increases gradually to the value of the homogeneous film with the increase of current density J . Our theory (red line) captures well this trend.

How to manipulate and control skyrmion Hall angle is an important issue in device applications because non-zero Hall angle tends to pushes skyrmions to sample edges, leading to skyrmion annihilation. Even though the Hall effect itself comes from skyrmion topological structure that seems have nothing to do with disorders, two independent experiments showed recently that the skyrmion Hall angle ($\theta_{\text{SH}} \equiv \arctan(v_y/v_x)$) first increases with current density and then saturates at a sufficiently large value^{32,34}. So far, a good understanding of the observed behavior of Spin Hall angle is still lacking although there are simulations^{38,46} showing the saturation behavior. So far, most theoretical studies considered only isolated defects. Although isolated defects are important in real systems, systems with continuous random grain boundaries may be more relevant for amorphous and poly-crystal films^{44,46}.

It should be useful to compare our findings with recent works. Ref.³⁹ treats skyrmions as point-particles and artificially treats disorder effect as a harmonic potential on skyrmions. This assumption is not well justified and its prediction cannot compare against micromagnetic simulations and experiments. In contrast, our random force expression is well justified and compared with simulations. The resulting results for the skyrmion Hall angle describe well both STT and SOT driving skyrmions that have opposite current dependence. Ref.⁴⁷ is on the interaction of skyrmions with atomic defects in PdFe/Ir and it is different from what we have done here. Also, the first-principles calculations are more like experiments that do not automatically provide the physics. As an example, the reference did not obtain the random force reported here. Moreover, the dynamics of skyrmion as well as the skyrmion Hall effect were not studied in the mentioned paper.

In conclusion, we have investigated the skyrmion motion in inhomogeneous magnetic films. Three phases are identified: They are pinning phase when the disorder strength is above a critical value that depends on the driving current density. Below the critical disorder strength, the skyrmion transverse motion is boosted by the disorder below a critical damping while the transverse motion is hindered above the critical damping. The crit-

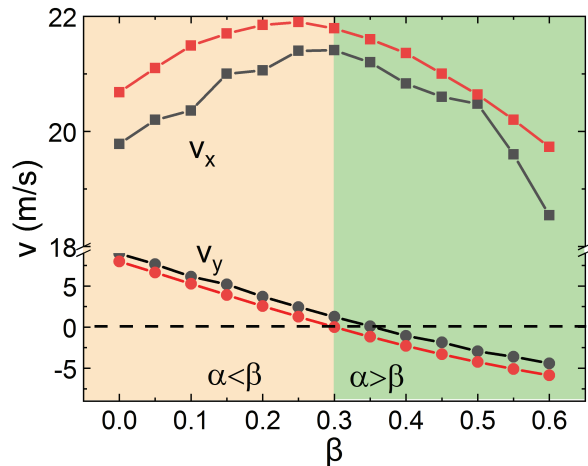


FIG. 9. (color online) The β -dependence of longitudinal (squares) and transverse (dots) velocities for $\alpha = 0.3$, $J = 6 \times 10^{11} \text{ A/m}^2$ and $\Delta K = 3\% K_0$. The red colors denote the velocities in the homogeneous film while the black colors are for the granular film.

ical damping depends also on the current density and the disorder strength. We showed that boosting of the transverse motion is mainly due to the random force opposite to the current direction. We further demonstrated that the generalised Thiele equation can perfectly capture skyrmion dynamics with a random force. Similar to the friction force in Newtonian mechanics in which there exist static and kinetic friction forces, the random force on a skyrmion can be classified as the static random force and kinetic random force. For a pinned skyrmion, the static force is always transverse to the current direction such that random force balances the current driving force $\vec{G} \times \vec{u}$, where \vec{u} is the usual quantity that characterise the Slonczewski spin-transfer torque. When the skyrmion is in motion, the direction of the kinetic random force is opposite to the skyrmion velocity, and the value of the kinetic random force is proportional to the $(\Delta K)^2/u$.

V. ACKNOWLEDGEMENT

This work is supported by by the NSFC Grant (No. 11974296 and 11774296) and Hong Kong RGC Grants (No. 16301518, 16301619 and 16300117). HYY was financially supported by National Natural Science Foundation of China (Grants No. 61704071).

VI. APPENDIX

In this appendix, we show further reduce mesh size below 1 nm will not change simulation results within model parameters used. We simulate the skyrmion velocity using different mesh size, as shown in Fig. 10. When mesh

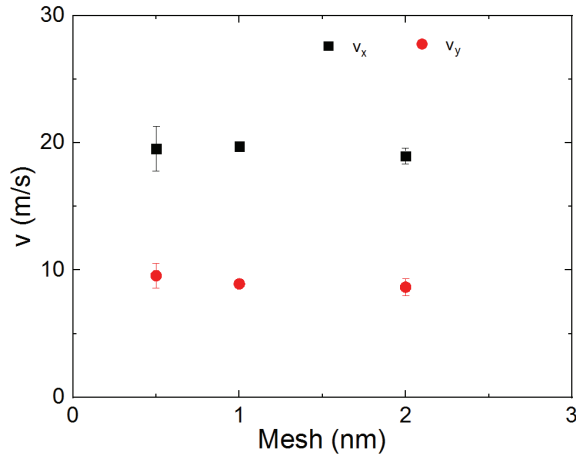


FIG. 10. (color online) The mesh size dependence of skyrmion velocities for $J = 6 \times 10^{11} \text{ A/m}^2$ and $\Delta K = 3\%K_0$, $\alpha = 0.3$.

is larger than 4 nm, the skyrmion is unstable. As mesh decreases from 2 nm to 0.5 nm, the skyrmion velocity does not change significantly. This indicates that 1 nm mesh used in the main text is sufficient.

-
- * Electronic address: yuanhy@sustech.edu.cn
† Electronic address: phxwan@ust.hk
- ¹ A. N. Bogdanov and U. K. Röbner, Phys. Rev. Lett. **87**, 037203 (2001).
 - ² U. K. Röbner, A. N. Bogdanov, and C. Pfleiderer, Nature **442**, 797 (2006).
 - ³ S. Mühlbauer, B. Binz, F. Jonietz, C. Pfleiderer, A. Rosch, A. Neubauer, G. Georgii, and P. Böni, Science **323**, 915 (2009).
 - ⁴ N. Romming, C. Hanneken, M. Menzel, J. E. Bickel, B. Wolter, K. von Bergmann, A. Kubetzka, and R. Wiesendanger, Science **341**, 636 (2013).
 - ⁵ X. Z. Yu et al., Nature **465**, 901 (2010).
 - ⁶ X. Z. Yu et al., Nat. Mater. **10**, 106 (2011).
 - ⁷ Y. Zhou, and M. A. Ezawa, Nat. Commun. **5**, 4652 (2014).
 - ⁸ H. Y. Yuan and X. R. Wang, Sci. Rep. **6**, 22638 (2016).
 - ⁹ Y. Onose, Y. Okamura, S. Seki, S. Ishiwata, and Y. Tokura, Phys. Rev. Lett. **109**, 037603 (2012).
 - ¹⁰ H. S. Park, X. Z. Yu, S. Aizawa, T. Tanikaki, T. Akashi, Y. Takahashi, T. Matsuda, N. Kanazawa, Y. Onose, D. Shindo, A. Tonomura, and Y. Tokura, Nat. Nanotech. **9**, 337 (2014).
 - ¹¹ H. Du, R. Che, L. Kong, X. Zhao, C. Jin, C. Wang, J. Yang, W. Ning, R. Li, C. Jin, X. Chen, J. Zang, Y. Zhang, and M. Tian, Nat. Commun. **6**, 8504 (2015).
 - ¹² S. Heinze, K. von Bergmann, M. Menzel, J. Brede, A. Kubetzka, R. Wiesendanger, G. Bihlmayer, and Stefan Blügel Nat. Phys. **7**, 713-718 (2011).
 - ¹³ W. Jiang, P. Upadhyaya, W. Zhang, G. Yu, M. B. Jungfleisch, F. Y. Fradin, J. E. Pearson, Y. Tserkovnyak, K. L. Wang, O. Heinonen, S. G. E. te Velthuis, and A. Hoffmann, Science **349**, 283 (2015).
 - ¹⁴ J. Li, A. Tan, K. W. Moon, A. Doran, M. A. Marcus, A. T. Young, E. Arenholz, S. Ma, R. F. Yang, C. Hwang, and Z. Q. Qiu, Nat. Commun. **5**, 4704 (2014).
 - ¹⁵ S. Krause and R. Wiesendanger, Nat. Mater. **15**, 493 (2016).
 - ¹⁶ N. Nagaosa, and Y. Tokura, Nat. Nanotech. **8**, 899 (2013).
 - ¹⁷ A. Fert, V. Cros, and J. Sampaio, Nat. Nanotech. **8**, 152 (2013); J. Sampaio, V. Cros, S. Rohart, A. Thiaville, and A. Fert, *ibid.* **8**, 839 (2013).
 - ¹⁸ P. Dürrenfeld, Y. Xu, J. Åkerman, and Y. Zhou, Phys. Rev. B **96**, 054430 (2017).
 - ¹⁹ L. Kong and J. Zang, Phys. Rev. Lett. **111**, 067203 (2013).
 - ²⁰ S. Rohart and A. Thiaville, Phys. Rev. B **88**, 184422 (2013).
 - ²¹ M. N. Wilson, A. B. Butenko, A. N. Bogdanov, and T. L. Monchesky, Phys. Rev. B **89**, 094411 (2014).
 - ²² N. Romming, A. Kubetzka, C. Hanneken, K. von Bergmann, and R. Wiesendanger, Phys. Rev. Lett. **114**, 177203 (2015).
 - ²³ M. A. Castro and S. Allende, J. Magn. Magn. Mater. **417**, 344 (2016).
 - ²⁴ X. S. Wang, H. Y. Yuan, and X. R. Wang, Communications Physics **1**, 31 (2018).
 - ²⁵ N. Vidal-Silva, A. Riveros, and J. Escrig, J. Magn. Magn. Mater. **443**, 116 (2017).
 - ²⁶ A. O. Lenov, T. L. Monchesky, N. Romming, A. Kubetzka, A. N. Bogdanov, and R. Wiesendanger, New J. Phys. **18**, 065003 (2016).
 - ²⁷ H.-B. Braun, Phys. Rev. B **50**, 16485 (1994).
 - ²⁸ A. Siemens, Y. Zhang, J. Hagemeister, E. Y. Vedmedenko, and R. Wiesendanger, New J. Phys. **18**, 045021 (2016).
 - ²⁹ E. Simon, K. Palotás, L. Rózsa, L. Udvardi, and L. Szunyogh, Phys. Rev. B **90**, 094410 (2014).
 - ³⁰ S. Jaiswal, K. Litzius, I. Lemes, F. Bttner, S. Finizio, J. Raabe, M. Weigand, K. Lee, J. Langer, B. Ocker, G. Jakob, G. S. D. Beach, and M. Kläui, Appl. Phys. Lett. **111**, 022409 (2017).
 - ³¹ E. A. Karhu, U. K. Röbner, A. N. Bogdanov, S. Kahwaji, B. J. Kirby, H. Fritzsche, M. D. Robertson, C. F. Majkrzak, and T. L. Monchesky, Phys. Rev. B **85**, 094429 (2012).
 - ³² W. Jiang, X. Zhang, G. Yu, W. Zhang, X. Wang, M. B. Jungfleisch, J. E. Pearson, X. Cheng, O. Heinonen, K. L. Wang, Y. Zhou, A. Hoffmann, and S. G. E. te Velthuis, Nat. Phys. **13**, 162 (2017).

- ³³ H. Y. Yuan, O. Gomonay, and M. Klaui, *Phys. Rev. B* **96**, 134415 (2017).
- ³⁴ K. Litzius et al., *Nat. Phys.* **13**, 170 (2017).
- ³⁵ H. Y. Yuan, X.S. Wang, Man-Hong Yung, and X. R. Wang, *Phys. Rev. B* **99**, 014428 (2019).
- ³⁶ S. Woo, K. Litzius, B. Krüger, M.-Y. Im, L. Caretta, K. Richter, M. Mann, A. Krone, R. M. Reeve, M. Weigand, P. Agrawal, I. Lemesch, M.-A. Mawass, P. Fischer, M. Kläui, and G. S. D. Beach, *Nat. Mater.* **15**, 501 (2016).
- ³⁷ J. Iwasaki, M. Mochizuki, and N. Nagaosa, *Nat. Commun.* **4**, 1463 (2013).
- ³⁸ C. Reichhardt, D. Ray, and C. J. Olson Reichhardt, *Phys. Rev. Lett.* **114**, 217202 (2015).
- ³⁹ C. Reichhardt and C. J. Olson Reichhardt, *New J. Phys.* **18**, 095005 (2016).
- ⁴⁰ J. Sampaio, V. Cros, S. Rohart, A. Thiaville and A. Fert, *Nat. Nanotech.* **8**, 839 (2013).
- ⁴¹ S.-Z. Lin, C. Reichhardt, C. D. Batista, and A. Saxena, *Phys. Rev. B* **87**, 214419 (2013).
- ⁴² W. Koshibae and N. Nagaosa, *Sci. Rep.* **8**, 6238 (2018).
- ⁴³ R. Juge et al., *J. Magn. Magn. Mater.* **455**, 3 (2018).
- ⁴⁴ J.-V. Kim and M. -W. Yoo, *Appl. Phys. Lett.* **110**, 132404 (2018).
- ⁴⁵ S. Hoshino and N. Nagaosa, *Phys. Rev. B* **97**, 024413 (2018).
- ⁴⁶ S. Woo et al., *Nat. Commun.* **9**, 959 (2018).
- ⁴⁷ I. L. Fernandes, J. Bouaziz, S. Blügel, and S. Lounis, *Nat. Commun.* **9**, 4395 (2018).
- ⁴⁸ R. Juge, S.-G. Je, D. de Souza Chaves, L. D. Buda-Prejbeanu, J. Peña-Garcia, J. Nath, I. M. Miron, K. G. Rana, L. Aballe, M. Foerster, F. Geunuzio, T. O. Montes, A. Locatelli, F. Maccherozzi, S. S. Dhesi, M. Belmeguenai, Y. Roussigné, S. Auffret, S. Pizzini, G. Gaudin, J. Vogel, and O. Boulle, arXiv: 1904.08275v4.
- ⁴⁹ T. Nozaki et al., *Appl. Phys. Lett.* **114**, 012402 (2019).
- ⁵⁰ S. Zhang and Z. Li, *Phys. Rev. Lett.* **93**, 127204 (2004).
- ⁵¹ A. Thiaville, Y. Nakatani, J. Miltat, and Y. Suzuki, *Europhys. Lett.* **69**, 990 (2005).
- ⁵² A. Vansteenkiste, J. Leliaert, M. Dvornik, M. Helsen, F. Garcia-Sanchez, and F. B. V. Waeyenberge, *AIP Adv.* **4**, 107133 (2014).
- ⁵³ A. A. Thiele, *Phys. Rev. Lett.* **30**, 230 (1973).
- ⁵⁴ H.Y. Yuan and X.R. Wang, *Phys. Rev. B* **89**, 054423 (2014).
- ⁵⁵ H.Y. Yuan and X.R. Wang, *Phys. Rev. B* **92**, 054419 (2015).
- ⁵⁶ H.Y. Yuan and X.R. Wang, *Euro Phys. Journal B* **88**, 214 (2015).
- ⁵⁷ A. Salimath, A. Abbout, A. Brataas, A. Manchon, *Phys. Rev. B* **99**, 104416 (2019).
- ⁵⁸ G. Q. Yu, P. Upadhyaya, X. Li, W. Li, S. K. Kim, Y. Fan, K. L. Wong, Y. Tserkovnyak, P. K. Amiri, K. L. Wang, *Nano Lett.* **16**, 1981 (2016).